

Constraining models for the origin of ultra-high-energy cosmic rays with spectrum, composition, and arrival direction data measured at the Pierre Auger Observatory

Teresa Bister^{a,b,*} for the Pierre Auger Collaboration^c

^a*Institute for Mathematics, Astrophysics and Particle Physics, Radboud University Nijmegen Nijmegen, The Netherlands*

^b*Nationaal Instituut voor Kernfysica en Hoge Energie Fysica (NIKHEF), Science Park, Amsterdam, The Netherlands*

^c*Observatorio Pierre Auger, Av. San Martín Norte 304, 5613 Malargüe, Argentina
Full author list: https://www.auger.org/archive/authors_icrc_2023.html*

E-mail: spokespersons@auger.org

The distribution of cosmic-ray arrival directions shows a better agreement with models in which a fraction of the flux is associated with catalogs of nearby source candidates, such as starburst galaxies, than with isotropy. To investigate this further, we use a novel approach, fitting simultaneously the energy spectrum, distributions of shower maxima, and arrival directions at the highest energies measured with the Pierre Auger Observatory. The astrophysical model consists of homogeneously distributed background sources as well as an adaptable contribution from nearby source candidates. Propagation effects and a rigidity-dependent magnetic field blurring are taken into account, producing a rising level of anisotropy with the energy. We demonstrate that a model containing a flux fraction of around 20% from the starburst galaxy catalog at 40 EeV, with a hard, nitrogen-dominated injection spectrum, provides a good description of the data. By investigating a scenario with Cen A as a single source in combination with the homogeneous background, we show that this region of the sky provides the dominant part to the observed anisotropy signal. Models based on jetted active galactic nuclei whose cosmic-ray flux scales with the gamma-ray emission are disfavored. The modeled energy evolution of the arrival directions, the spectra of individual sources, as well as the statistical significance of the results, including the influence of experimental systematic effects, will be discussed in this contribution.

38th International Cosmic Ray Conference (ICRC2023)
26 July - 3 August, 2023
Nagoya, Japan



*Speaker

1. Introduction

Ultra-high-energy cosmic rays (UHECRs) persist as an area of profound investigation, with the quest to unveil their origin on the brink of realization. Recent findings indicate a potential correlation between UHECR arrival directions above 40 EeV and the directions of powerful extragalactic source candidates [1, 2]. Several catalogs have been tested, including selections of jetted active galactic nuclei (γ -AGNs) and starburst galaxies (SBGs). While the statistical significance is highest for the selection of SBGs with 3.8σ [3], the presence of several different strong sources in the Centaurus region makes it difficult to favor any specific catalog at present. In a separate study, the excess in the Centaurus region, centered on the nearby radio galaxy Cen A, is determined to 4.0σ significance [3].¹

Previous analyses by the Pierre Auger Collaboration have leveraged the energy spectrum and shower maximum depth distributions to constrain generic source models of UHECRs [4, 5]. Building upon this foundation, the present work conducts a comprehensive investigation by simultaneously fitting the energy spectrum, shower maximum distributions, and additionally the arrival directions measured at the Pierre Auger Observatory. With this approach, parameters describing the source setup and emission are determined. We employ a straightforward astrophysical model based on the observed medium-scale anisotropies at the highest energies, correlated with extragalactic objects. In the model, propagation effects, as well as a rigidity-dependent blurring as expected from interaction with (mostly) turbulent magnetic fields, are considered. We use the following data sets: the arrival direction data >16 EeV from [2], the energy spectrum >10 EeV from [6], and the shower maximum distributions >10 EeV from [7].

A preliminary proof of concept for this method, utilizing realistic simulations, has been presented in [8, 9]. In an upcoming publication, the method and results are described in detail [10].

2. Astrophysical model and combined fit

The astrophysical model consists of two parts, the sources from either the SBG / γ -AGN catalogs from [2] or Cen A as a single source, in addition to a homogeneous background. The background evolution is modeled as $\propto (1+z)^m$, where either $m = 0$ (flat), $m = 3.4$ (star formation rate, SFR) or $m = 5.0$ (γ -AGNs). All sources accelerate CRs to a maximum rigidity R_{cut} , so that the generation rate Q_{inj} (per unit of energy, volume, and time) follows a power law with a broken exponential cutoff:

$$Q_{\text{inj}}(E_{\text{inj}}, A_{\text{inj}}) = Q_0 a_A \left(\frac{E_{\text{inj}}}{10^{18} \text{ eV}} \right)^{-\gamma} \cdot \begin{cases} 1, & Z_A R_{\text{cut}} > E_{\text{inj}}; \\ \exp \left(1 - \frac{E_{\text{inj}}}{Z_A R_{\text{cut}}} \right), & Z_A R_{\text{cut}} \leq E_{\text{inj}}; \end{cases} \quad (1)$$

Here, γ is the spectral index, a_A is the contribution of each representative element (H, He, N, Si, Fe) at a fixed energy below R_{cut} , and Q_0 is a normalization for the UHECR generation rate. In practice, instead of a_A we use the integral fraction $I_A = a_A Z_A^{2-\gamma} / (\sum_A a_A Z_A^{2-\gamma})$ for a more stable fit.

To take into account the effects of propagation, namely the interactions with background photon fields, we generate a database of 1-dimensional CRPropa [11] simulations (for specifics see [10]).

¹Note that in this work we use a data set including events up to 31 Dec 2020 [2] (rather than up to 31 Dec 2022 [3]), on which the one-sided significance for the correlation with SBGs was 4.0σ , and 3.9σ for the Centaurus region.

We utilize the Gilmore model [12] for the extragalactic background light and TALYS [13] to model the photodisintegration.

The catalog sources are positioned at their respective distances, and their relative flux is weighted based on the flux weights from [2], which are based on astrophysical measurements (the radio flux for SBGs and the γ -ray flux for the γ -AGNs). The background and catalog contributions are then combined by weighting them with a signal fraction f_0 . This signal fraction is defined for the energy bin $10^{19.5} - 10^{19.6}$ eV (≈ 40 EeV for comparability to [1, 2]). It is important to note that the *catalog contribution* $f_S(f_0, E_{\text{det}}^e)$ as a function of energy is fully determined by propagation effects, and will usually be larger at higher energies due to propagation effects. The *signal fraction* f_0 is used to fix the absolute scale of that contribution at a fixed energy.

From the arriving UHECRs, we compute probability distributions binned in energy for all three observables, where detector effects are taken into account. For the energy and X_{max} distributions, we use the same approach and binning as in [4]. For X_{max} specifically, we calculate the expected probability distribution using Gumbel distributions [14] with the EPOS-LHC hadronic interaction model. For the arrival directions, we generate a probability map (pdf) in each energy bin. To model the effects expected by mostly turbulent magnetic fields, we introduce Fisher distributions around each catalog source with a width $\delta_S = \delta_0 Z_{\text{det}} \frac{10 \text{ EeV}}{E_{\text{det}}}$, where Z_{det} takes on values of 1, 2, 7, 14, and 26 for $A_{\text{det}} \in \{1\}, \{2, 3, 4\}, \{5, \dots, 22\}, \{23, \dots, 38\}$ and $\{39, \dots, 56\}$, respectively. Each Fisher distribution is weighted by the directional exposure, as well as the number of arriving events with the corresponding charge Z_{det} in the energy bin E_{det} , which depends on the source weight and distance. The background probability map follows the directional exposure, assuming an isotropic distribution of background sources located at greater distances. Using the signal contribution function f_S introduced above, this leads to the energy-dependent pdfs:

$$\text{pdf}(E_{\text{det}}^e, \text{pix}^P) = f_S(f_0, E_{\text{det}}^e) S(E_{\text{det}}^e, \text{pix}^P) + (1 - f_S(f_0, E_{\text{det}}^e)) B(\text{pix}^P) := \text{pdf}^{e,P} \quad (2)$$

The pdf, as well as the signal and background maps S and B are binned into healpy [15] pixels pix^P .

Fit method: In total, the model has 9 free model parameters: γ , R_{cut} , four out of five element fractions I_a (subject to the condition $\sum_a I_a = 1$), Q_0 , δ_0 , and f_0 . Additionally, we include possible systematic shifts of the energy and X_{max} scales as nuisance parameters ν_E and $\nu_{X_{\text{max}}}$,² here in units of standard scores. The hadronic interaction model has a significant impact on the fit results, which can be partially captured by a shift of the X_{max} scale.

To determine the fit parameters, we use both a Bayesian sampler and a gradient-based minimizer (see [10]). For the systematic uncertainties included as nuisance parameters, we use a Gaussian likelihood $\log \mathcal{L}_{\text{syst}}$. The likelihood function for the measured energy spectrum $\log \mathcal{L}_E$ is modeled as a Poisson distribution, and the X_{max} likelihood $\log \mathcal{L}_{X_{\text{max}}}$ follows a multinomial distribution, as in [4, 5, 10]. For the arrival directions, we employ a similar likelihood function as in [1, 2], but bin the events $n^{e,P}$ into detected energy bins e and pixels p and utilize the modeled energy-dependent probability maps pdf^e from eq. 2:

$$\mathcal{L}_{\text{ADs}} = \prod_e \prod_p (\text{pdf}^{e,p})^{n^{e,p}} \quad (3)$$

²In [5], we show results for both free nuisance parameters for the experimental systematic uncertainties, as well as for fixed $\nu_{X_{\text{max}}} = \nu_E = 0$. In this work, we focus on the first case.

	Cen A, $m = 0$ (flat)		Cen A, $m = 3.4$ (SFR)		SBG, $m = 3.4$ (SFR)	
	posterior	MLE	posterior	MLE	posterior	MLE
γ	$-0.89^{+0.37}_{-0.33}$	-0.65	$-1.19^{+0.45}_{-0.39}$	-1.41	$-1.02^{+0.43}_{-0.36}$	-1.25
$\log_{10}(R_{\text{cut}}/\text{V})$	$18.20^{+0.04}_{-0.05}$	18.23	$18.21^{+0.04}_{-0.05}$	18.20	$18.24^{+0.04}_{-0.06}$	18.22
f_0	$0.07^{+0.01}_{-0.05}$	0.029	$0.07^{+0.01}_{-0.05}$	0.031	$0.19^{+0.07}_{-0.11}$	0.23
$\delta_0/^\circ$	$30.5^{+2.0}_{-20.2}$	14.4	$27.4^{+4.2}_{-17.0}$	14.3	$18.8^{+5.9}_{-3.6}$	21.9
I_{H}	$5.8^{+2.9}_{-2.6} \times 10^{-2}$	4.2×10^{-4}	$1.2^{+0.2}_{-1.2} \times 10^{-2}$	3.0×10^{-4}	$1.2^{+0.1}_{-1.2} \times 10^{-2}$	1.0×10^{-4}
I_{He}	$2.7^{+0.4}_{-0.4} \times 10^{-1}$	3.5×10^{-1}	$9.9^{+3.8}_{-2.9} \times 10^{-2}$	1.2×10^{-1}	$1.1^{+0.3}_{-0.4} \times 10^{-1}$	1.4×10^{-1}
I_{N}	$5.6^{+0.4}_{-0.4} \times 10^{-1}$	5.0×10^{-1}	$6.7^{+0.7}_{-0.7} \times 10^{-1}$	6.8×10^{-1}	$7.2^{+0.6}_{-0.6} \times 10^{-1}$	7.3×10^{-1}
I_{Si}	$9.0^{+3.9}_{-3.4} \times 10^{-2}$	1.4×10^{-1}	$1.5^{+0.5}_{-0.6} \times 10^{-1}$	1.6×10^{-1}	$1.2^{+0.5}_{-0.5} \times 10^{-1}$	9.8×10^{-2}
I_{Fe}	$2.3^{+0.9}_{-1.2} \times 10^{-2}$	1.8×10^{-2}	$5.1^{+1.5}_{-1.8} \times 10^{-2}$	4.4×10^{-2}	$4.7^{+1.3}_{-1.7} \times 10^{-2}$	3.8×10^{-2}
ν_E/σ	$-1.24^{+0.68}_{-0.50}$	-1.35	$0.23^{+0.42}_{-0.60}$	0.13	$0.35^{+0.44}_{-0.65}$	0.40
$\nu_{X_{\text{max}}}/\sigma$	$-0.94^{+0.29}_{-0.24}$	-0.97	$-1.60^{+0.30}_{-0.25}$	-1.45	$-1.55^{+0.26}_{-0.25}$	-1.33
D_{syst}		2.8		2.1		1.9
D_E ($N_J = 14$)		13.6		21.9		25.3
$D_{X_{\text{max}}}$ ($N_{X_{\text{max}}} = 74$)		107.4		113.6		112.7
$D_{\text{syst}} + D_E + D_{X_{\text{max}}}$		123.8		137.7		139.9
$\log \mathcal{L}_{\text{ADs}}$		9.4		9.5		13.5
$\log \mathcal{L}_{\text{tot}}$		-228.51		-235.3		-232.4
TS_E		-1.4		-1.1		-4.5
$\text{TS}_{X_{\text{max}}}$		0.2		1.0		2.0
TS_{ADs}		18.7		19.0		27.1
TS_{tot}		17.3		19.1		25.6

Table 1: Fit results for the Cen A and SBG models: the best-fit (MLE) parameters and the corresponding deviance $D = -2(\log \mathcal{L} - \log \mathcal{L}_{\text{saturated}})$ (see [4]) and log-likelihood values $\log \mathcal{L}$ are stated. Also, the posterior mean and highest posterior density interval obtained from a Bayesian sampler are given.

Since the observables are independent measurements, the total likelihood function is the product of the individual likelihood functions: $\log \mathcal{L}_{\text{tot}} = \log \mathcal{L}_E + \log \mathcal{L}_{X_{\text{max}}} + \log \mathcal{L}_{\text{ADs}} + \log \mathcal{L}_{\text{syst}}$.

In our analysis, we include only $E_{\text{det}} > 10$ EeV for both spectrum and X_{max} data. We expect contributions from sources other than our catalog sources below this energy threshold, such as Galactic or lower-energy extragalactic source classes, as supported by the findings in [5]. However, we also ensure that our model does not produce a larger flux below this threshold than measured by Auger through a one-sided spectrum likelihood below 10 EeV. For the arrival directions, we set an energy threshold at 16 EeV, as we do not intend to model the observed dipole in the arrival directions that is strongest around 8 EeV [3] with our model.

3. Results

In table 1, the best-fit parameters obtained from the gradient-based minimizer, as well as the posterior mean values including uncertainties from the Bayesian sampler, are provided for the SBG and Cen A models. The corresponding fitted spectra and moments of the shower maximum distributions are depicted in figure 1. Notably, the spectral index $\gamma \approx -1$ is hard for all models (note minus sign in eq. 1), while the maximum rigidity is relatively small with $\log_{10}(R_{\text{cut}}/\text{V}) \approx 18.2$. Note that especially the spectral index is very sensitive to the uncertainty on the X_{max} scale (see [10]), which is determined to be around $\nu_{X_{\text{max}}} = -1.5\sigma$, corresponding to a heavier true composition than

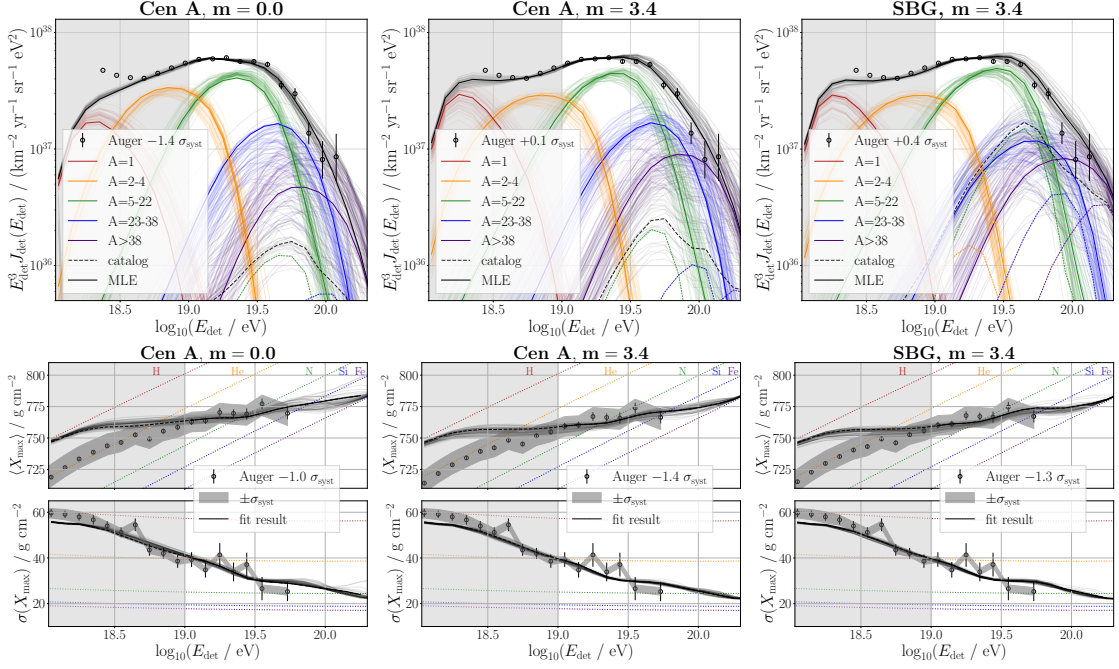


Figure 1: Modeled spectra (upper row) and X_{max} moments (lower row) on Earth for the Cen A model with $m = 0$ (left), $m = 3.4$ (middle) and the SBG model with $m = 3.4$ (right). The thick lines indicate the best fit, the thin lines are drawn from the posterior distribution demonstrating the uncertainty. The markers represent the measured data of the Pierre Auger Observatory. The grey area symbolizes the energy bins which are not (fully) included in the fit. The contribution of the source catalog is indicated by the dashed line in the spectrum. The data are shifted by the best-fit values for the energy / X_{max} scale as stated in table 1.

measured. The magnetic field blurring is $\delta_0 \approx 20^\circ$ for the SBG model. For the Cen A model, the blurring value is in agreement with that (note however the skewed posterior uncertainty). The signal fraction is around $f_0 \approx 20\%$ for the SBG model. For the Cen A model, the best-fit signal fraction is $f_0 \approx 3\%$ (again with the posterior implying that larger values are also possible). When calculating the signal contribution of NGC 4945 (the strongest source in the SBG catalog, located in the Centaurus region and with a similar distance of ≈ 4 Mpc) to the total contribution of the SBG catalog, a similar value of around 3% is observed. This implies that the contribution of a possible source in the Centaurus region with a distance of around 4 Mpc is consistently fitted independent of the background evolution, systematics (see [10]), and the possible influence of further sources in the catalog. To verify that the measured data in the Centaurus region is in fact well described by this source, we visualize the spectrum in a 20° radius window around Cen A / NGC 4945 in figure 2, both for the measured data as well as for the model. It is found that the reduced χ^2 for the model around the source candidate region is smaller than that of the whole sky by around 10% to 40% for all tested angles between 5° and 30° .

The modeled arrival directions are depicted in figure 3 for three example energy bins. Here, it is explicitly visible how the Centaurus region is fitted consistently regarding both blurring and signal fraction. Also, other things can be observed: the level of anisotropy rises with the energy as the relative influence of the close-by catalog sources increases due to propagation effects. Overall,

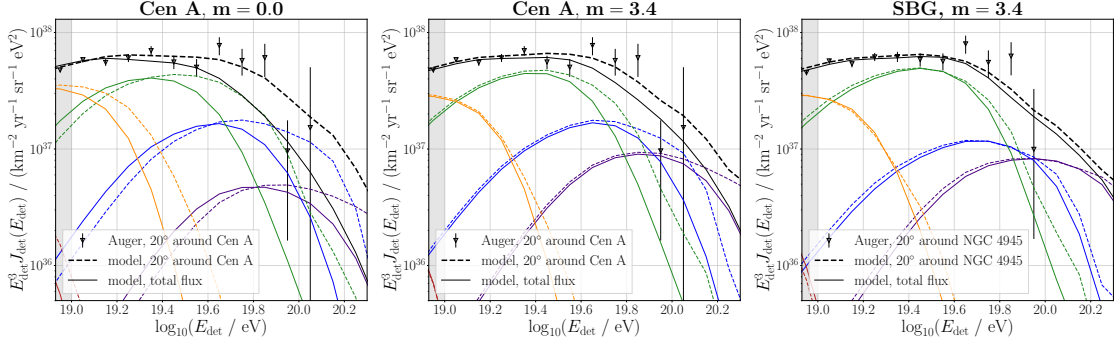


Figure 2: Spectra on Earth inside a circular region with 20° radius around the direction of Cen A (*left and middle*) or NGC 4945 (*right*). The colors are the same as in figure 1. The markers represent the measured data from the Pierre Auger Observatory inside the 20° region, the dashed lines the best-fit model in that region, and the solid lines the full-sky best-fit model as in figure 1.

the size of the blurring stays almost constant with the energy, which is a result of the almost constant rigidity due to the hard spectral index. The fitted arrival directions are almost independent of the experimental systematic uncertainties on energy and X_{\max} scale (compare to [10]).

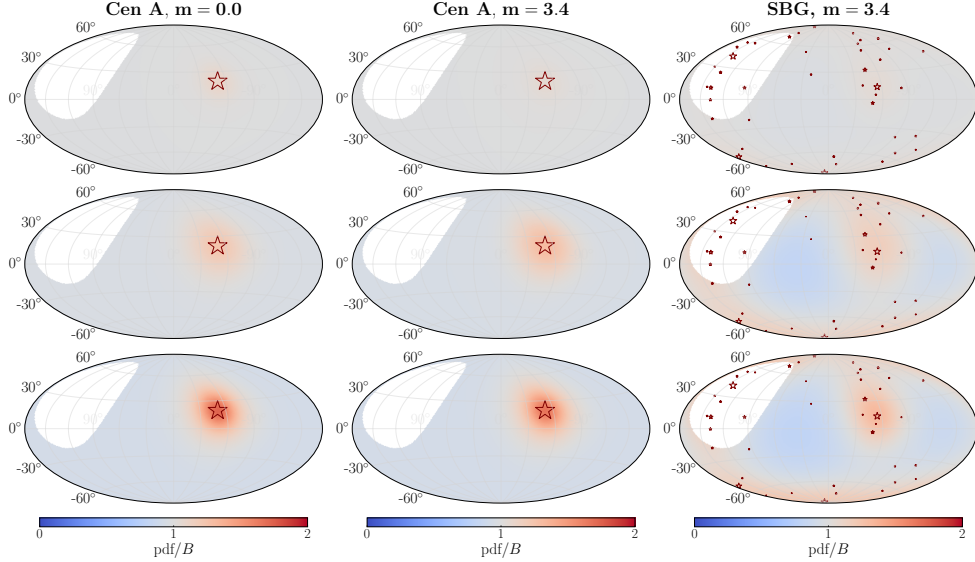


Figure 3: Modeled arrival directions pdf (eq. 2). The energy bins $\log_{10}(E_{\text{det}}/\text{eV}) = 19.3$ (*upper row*), $\log_{10}(E_{\text{det}}/\text{eV}) = 19.6$ (*middle row*) and $\log_{10}(E_{\text{det}}/\text{eV}) = 19.9$ (*lower row*) are shown exemplarily. The stars indicate the directions of the source candidates with the size scaling with the relative flux contribution before the exposure of the Observatory is accounted for. Note that the best-fit value for δ_0 used in these figures for the Cen A model is small compared to the posterior mean.

Test statistic: To quantify how well each tested model describes the measured data, the values of the likelihood can be compared. From table 1 it becomes clear that the Cen A model with flat evolution is the best fit, which comes mainly because the flat background evolution describes the data better than the SFR one (see [10]). To compare just the improvement from adding catalog sources

independently of the background source evolution, the test statistic can be used. It is defined as twice the log-likelihood ratio between a model and its respective reference model (only homogeneous background sources with the same source evolution, for fit values see [10]). The values for the test statistic for each model are provided in table 1 (lower rows). The largest test statistic is reached for the starburst galaxy model with $TS_{\text{tot}} = 25.6$. Using a χ^2 distribution with two degrees of freedom for the two additional fit parameters f_0 and δ_0 of the source model compared to the reference model, this amounts to a significance of 4.5σ . For the Cen A models, the test statistic is around $TS_{\text{tot}} \approx 20$, confirming that the Centaurus region provides

the most important contribution to the observed intermediate-scale anisotropies [2]. Notably, the arrival directions observable contributes most to the total test statistic, making it valuable to distinguish between different models. This aligns with expectations from simulation studies [8]. However, it is important to be cautious when interpreting the contributions of the three observables to the total TS values, as their relative size can vary considerably [9]. The arrival directions test statistic for each energy bin is shown in figure 4. It is important to note that for the present analysis, no scan of the energy threshold is necessary as in [1, 2] that would have to be penalized for. Instead, the whole energy dependency of the signal is considered in the model, so that a sum over all energy bins depicted in figure 4 leads to the total test statistic given in table 1.

The γ -AGN model: In figure 4, also the arrival directions test statistic obtained for a model based on γ -AGNs is depicted. For that model, the arrival directions test statistic is negative, indicating that the measured arrival directions are not described. The reason for that is the dominance of the faraway blazar Markarian 421 ($d \approx 140$ Mpc) in the model, due to the scaling of the flux weights with the γ -ray emission, that is not observed in the data.

We tested the influence of a possible distance-dependent blurring in addition to the rigidity-dependent one, as would be expected from turbulent extragalactic magnetic fields. Then, the best-fit blurring is very large, indicating the need for extremely strong extragalactic magnetic field strengths³ to counteract the dominance of Markarian 421. In that case, only Cen A is still visible in the arrival directions as it is the strongest closeby source in the γ -AGN catalog. As can be seen in figure 4, the arrival directions are now better described, but nevertheless still not as well as when Cen A is just taken as a single source. Hence, it can be concluded that a scaling of the UHECR

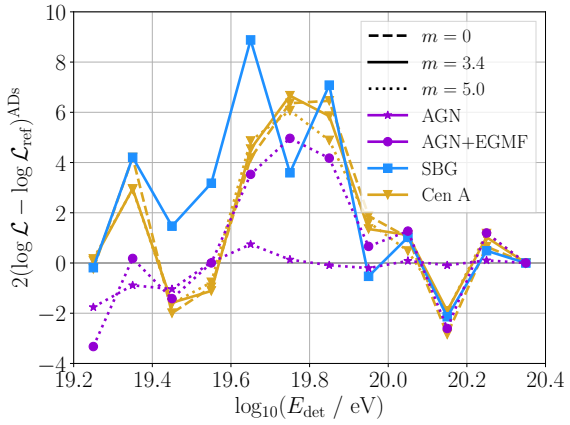


Figure 4: Arrival directions test statistic as a function of the energy bin for the tested source classes and evolutions. The test statistic is always calculated compared to the reference model with the same evolution. The sum over all energy bins corresponds to the values for TS_{ADs} given in table 1.

³The distance-dependent blurring can be constrained to $\gtrsim 5^\circ \sqrt{d_s/\text{Mpc}} 10 \text{ EV}/R$ for the γ -AGN model, indicating a magnetic field strength B and coherence length l_c that would have to fulfill $B\sqrt{l_c} \gtrsim nG\sqrt{\text{Mpc}}$ in that case.

intensity with the γ -ray flux for a γ -AGN source model is disfavored by the data measured at the Pierre Auger Observatory.

4. Conclusion

In this work, a possible origin of the observed correlations between the arrival directions of UHECRs and catalogs of extragalactic objects was investigated. For that, we performed a combined fit of the energy spectrum, shower maximum depth distributions, and arrival directions, considering propagation effects and an energy-dependent modeling of source contributions.

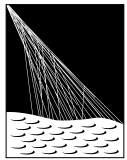
The largest test statistic (indicating how much the likelihood improves by adding catalog sources, compared to the reference model with only homogeneous background) was found for the model incorporating starburst galaxies. It amounts to 25.6 when experimental systematic uncertainties are considered, corresponding to a significance of 4.5σ . The best fit is reached with a hard spectral index, a signal fraction of approximately 20% at 40 EeV, and a blurring of around 20° at 10 EV rigidity. A separate investigation of a model with Cen A as the sole source resulted in a test statistic of around 20, independently of systematics and the background source evolution. We demonstrated that the observed overdensity in the Centaurus region is well described by both NGC 4945 in the starburst galaxy model, as well as Cen A, where in both cases the contribution of the respective source to the total flux is around 3% at 40 EeV. The γ -AGN model, previously showing correlations with arrival directions, does not agree well with the energy-dependent modeling of the arrival directions in this work due to the strong contribution of the distant blazar Markarian 421. Thus, it can be concluded that a scenario where the UHECR flux scales with the γ -ray intensity is disfavored.

Future extensions for this analysis could include investigating the effect of coherent deflections by the regular part of the Galactic magnetic field, exploring other source catalogs and lower energies, and leveraging the AugerPrime upgrade to the Pierre Auger Observatory for improved sensitivity and analysis capabilities.

References

- [1] A. Aab *et al.* [Pierre Auger coll.], ApJL **853** (2018) L29
- [2] P. Abreu *et al.* [Pierre Auger coll.], ApJ **935** (2022) 170
- [3] G. Golup *et al.* [Pierre Auger coll.], PoS ICRC2023 (2023) 252
- [4] A. Aab *et al.* [Pierre Auger coll.], JCAP **04** (2017) 038
- [5] A. Abdul Halim *et al.* [Pierre Auger coll.], JCAP **05** (2023) 024
- [6] A. Aab *et al.* [Pierre Auger coll.], PRD **102** (2020) 062005
- [7] A. Yushkov *et al.* [Pierre Auger coll.], PoS ICRC2019 (2019) 482
- [8] T. Bister *et al.* [Pierre Auger coll.], PoS ICRC2021 (2021) 368
- [9] T. Bister *et al.* [Pierre Auger coll.], EPJ Web Conf. **283** (2023) 03008
- [10] A. Abdul Halim *et al.* [Pierre Auger coll.], submitted to JCAP, arXiv:2305.16693
- [11] R. Alves Batista *et al.*, JCAP **1605** (2016) 038
- [12] R. Gilmore *et al.*, MNRAS **422** (2012) 3189
- [13] A. Koning and D. Rochman, Nucl. Data Sheets **113** (2012) 2841
- [14] M. De Domenico *et al.*, JCAP **1307** (2013) 050
- [15] A. Zonca *et al.*, J. Open Source Softw. **4** (2019) 35

The Pierre Auger Collaboration



PIERRE
AUGER
OBSERVATORY

- A. Abdul Halim¹³, P. Abreu⁷², M. Aglietta^{54,52}, I. Allekotte¹, K. Almeida Cheminant⁷⁰, A. Almela^{7,12}, R. Aloisio^{45,46}, J. Alvarez-Muñiz⁷⁹, J. Ammerman Yebra⁷⁹, G.A. Anastasi^{54,52}, L. Anchordoqui⁸⁶, B. Andrada⁷, S. Andringa⁷², C. Aramo⁵⁰, P.R. Araújo Ferreira⁴², E. Arnone^{63,52}, J.C. Arteaga Velázquez⁶⁷, H. Asorey⁷, P. Assis⁷², G. Avila¹¹, E. Avocone^{57,46}, A.M. Badescu⁷⁵, A. Bakalova³², A. Balaceanu⁷³, F. Barbato^{45,46}, A. Bartz Mocellin⁸⁵, J.A. Bellido^{13,69}, C. Berat³⁶, M.E. Bertaina^{63,52}, G. Bhatta⁷⁰, M. Bianciotto^{63,52}, P.L. Biermann^h, V. Binet⁵, K. Bismarck^{39,7}, T. Bister^{80,81}, J. Biteau³⁷, J. Blazek³², C. Bleve³⁶, J. Blümner⁴¹, M. Boháčová³², D. Boncioli^{57,46}, C. Bonifazi^{8,26}, L. Bonneau Arbeletche²¹, N. Borodai⁷⁰, J. Brack^j, P.G. Brichetto Orchera⁷, F.L. Brieche⁴², A. Bueno⁷⁸, S. Buitink¹⁵, M. Buscemi^{47,61}, M. Büsken^{39,7}, A. Bwembya^{80,81}, K.S. Caballero-Mora⁶⁶, S. Cabana-Freire⁷⁹, L. Caccianiga^{59,49}, I. Caracas³⁸, R. Caruso^{58,47}, A. Castellina^{54,52}, F. Catalani¹⁸, G. Cataldi⁴⁸, L. Cazon⁷⁹, M. Cerda¹⁰, A. Cermenati^{45,46}, J.A. Chinellato²¹, J. Chudoba³², L. Chytka³³, R.W. Clay¹³, A.C. Cobos Cerutti⁶, R. Colalillo^{60,50}, A. Coleman⁹⁰, M.R. Coluccia⁴⁸, R. Conceição⁷², A. Condorelli³⁷, G. Consolati^{49,55}, M. Conte^{56,48}, F. Convenga⁴¹, D. Correia dos Santos²⁸, P.J. Costa⁷², C.E. Covault⁸⁴, M. Cristinziani⁴⁴, C.S. Cruz Sanchez³, S. Dasso^{4,2}, K. Daumiller⁴¹, B.R. Dawson¹³, R.M. de Almeida²⁸, J. de Jesús^{7,41}, S.J. de Jong^{80,81}, J.R.T. de Mello Neto^{26,27}, I. De Mitri^{45,46}, J. de Oliveira¹⁷, D. de Oliveira Franco²¹, F. de Palma^{56,48}, V. de Souza¹⁹, E. De Vito^{56,48}, A. Del Popolo^{58,47}, O. Deligny³⁴, N. Denner³², L. Deval^{41,7}, A. di Matteo⁵², M. Dobre⁷³, C. Dobrigkeit²¹, J.C. D'Olivo⁶⁸, L.M. Domingues Mendes⁷², J.C. dos Anjos, R.C. dos Anjos²⁵, J. Ebr³², F. Ellwanger⁴¹, M. Emam^{80,81}, R. Engel^{39,41}, I. Epicoco^{56,48}, M. Erdmann⁴², A. Etchegoyen^{7,12}, C. Evoli^{45,46}, H. Falcke^{80,82,81}, J. Farmer⁸⁹, G. Farrar⁸⁸, A.C. Fauth²¹, N. Fazzini^e, F. Feldbusch⁴⁰, F. Fenu^{41,d}, A. Fernandes⁷², B. Fick⁸⁷, J.M. Figueira⁷, A. Filipčič^{77,76}, T. Fitoussi⁴¹, B. Flaggs⁹⁰, T. Fodran⁸⁰, T. Fujii^{89,f}, A. Fuster^{7,12}, C. Galea⁸⁰, C. Galelli^{59,49}, B. García⁶, C. Gaudu³⁸, H. Gemmeke⁴⁰, F. Gesualdi^{7,41}, A. Gherghel-Lascu⁷³, P.L. Ghia³⁴, U. Giaccari⁴⁸, M. Giammarchi⁴⁹, J. Glombitzka^{42,8}, F. Gobbi¹⁰, F. Gollan⁷, G. Golup¹, M. Gómez Berisso¹, P.F. Gómez Vitale¹¹, J.P. Gongora¹¹, J.M. González¹, N. González⁷, I. Goos¹, D. Góra⁷⁰, A. Gorgi^{54,52}, M. Gottowik⁷⁹, T.D. Grubb¹³, F. Guarino^{60,50}, G.P. Guedes²², E. Guido⁴⁴, S. Hahn³⁹, P. Hamal³², M.R. Hampel⁷, P. Hansen³, D. Harari¹, V.M. Harvey¹³, A. Haungs⁴¹, T. Hebbeker⁴², C. Hojvat^e, J.R. Hörandel^{80,81}, P. Horvath³³, M. Hrabovský³³, T. Huege^{41,15}, A. Insolia^{58,47}, P.G. Isar⁷⁴, P. Janecek³², J.A. Johnsen⁸⁵, J. Jurysek³², A. Kääpä³⁸, K.H. Kampert³⁸, B. Keilhauer⁴¹, A. Khakurdikar⁸⁰, V.V. Kizakke Covilakam^{7,41}, H.O. Klages⁴¹, M. Kleifges⁴⁰, F. Knapp³⁹, N. Kunka⁴⁰, B.L. Lago¹⁶, N. Langner⁴², M.A. Leigui de Oliveira²⁴, Y Lema-Capeans⁷⁹, V. Lenok³⁹, A. Letessier-Selvon³⁵, I. Lhenry-Yvon³⁴, D. Lo Presti^{58,47}, L. Lopes⁷², L. Lu⁹¹, Q. Luce³⁹, J.P. Lundquist⁷⁶, A. Machado Payeras²¹, M. Majercakova³², D. Mandat³², B.C. Manning¹³, P. Mantsch^e, S. Marafico³⁴, F.M. Mariami^{59,49}, A.G. Mariazzi³, I.C. Mariş¹⁴, G. Marsella^{61,47}, D. Martello^{56,48}, S. Martinelli^{41,7}, O. Martínez Bravo⁶⁴, M.A. Martins⁷⁹, M. Mastrodicasa^{57,46}, H.J. Mathes⁴¹, J. Matthews^a, G. Matthiae^{62,51}, E. Mayotte^{85,38}, S. Mayotte⁸⁵, P.O. Mazur^e, G. Medina-Tanco⁶⁸, J. Meinert³⁸, D. Melo⁷, A. Menshikov⁴⁰, C. Merx⁴¹, S. Michal³³, M.I. Micheletti⁵, L. Miramonti^{59,49}, S. Mollerach¹, F. Montanet³⁶, L. Morejon³⁸, C. Morello^{54,52}, A.L. Müller³², K. Mulrey^{80,81}, R. Mussa⁵², M. Muzio⁸⁸, W.M. Namasaka³⁸, S. Negi³², L. Nellen⁶⁸, K. Nguyen⁸⁷, G. Nicora⁹, M. Niculescu-Oglizanu⁷³, M. Niechciol⁴⁴, D. Nitz⁸⁷, D. Nosek³¹, V. Novotny³¹, L. Nožka³³, A. Nucita^{56,48}, L.A. Núñez³⁰, C. Oliveira¹⁹, M. Palatka³², J. Pallotta⁹, S. Panja³², G. Parente⁷⁹, T. Paulsen³⁸, J. Pawlowsky³⁸, M. Pech³², J. Pěkala⁷⁰, R. Pelayo⁶⁵, L.A.S. Pereira²³, E.E. Pereira Martins^{39,7}, J. Perez Armand²⁰, C. Pérez Bertolli^{7,41}, L. Perrone^{56,48}, S. Petrera^{45,46}, C. Petrucci^{57,46}, T. Pierog⁴¹, M. Pimenta⁷², M. Platino⁷, B. Pont⁸⁰, M. Pothast^{81,80}, M. Pourmohammad Shahvar^{61,47}, P. Privitera⁸⁹, M. Prouza³², A. Puyleart⁸⁷, S. Querchfeld³⁸, J. Rautenberg³⁸, D. Ravignani⁷, M. Reininghaus³⁹, J. Ridky³², F. Riehn⁷⁹, M. Risso⁴⁴, V. Rizi^{57,46}, W. Rodrigues de Carvalho⁸⁰, E. Rodriguez^{7,41}, J. Rodriguez Rojo¹¹, M.J. Roncoroni⁷, S. Rossoni⁴³, M. Roth⁴¹, E. Roulet¹, A.C. Rovero⁴, P. Ruehl⁴⁴, A. Saftoiu⁷³, M. Saharan⁸⁰, F. Salamida^{57,46}, H. Salazar⁶⁴, G. Salina⁵¹, J.D. Sanabria Gomez³⁰, F. Sánchez⁷, E.M. Santos²⁰, E. Santos³²,

F. Sarazin⁸⁵, R. Sarmento⁷², R. Sato¹¹, P. Savina⁹¹, C.M. Schäfer⁴¹, V. Scherini^{56,48}, H. Schieler⁴¹, M. Schimassek³⁴, M. Schimp³⁸, F. Schlüter⁴¹, D. Schmidt³⁹, O. Scholten^{15,i}, H. Schoorlemmer^{80,81}, P. Schovánek³², F.G. Schröder^{90,41}, J. Schulte⁴², T. Schulz⁴¹, S.J. Sciutto³, M. Scornavacche^{7,41}, A. Segreto^{53,47}, S. Sehgal³⁸, S.U. Shivashankara⁷⁶, G. Sigl⁴³, G. Silli⁷, O. Sima^{73,b}, F. Simon⁴⁰, R. Smau⁷³, R. Šmídá⁸⁹, P. Sommers^k, J.F. Soriano⁸⁶, R. Squartini¹⁰, M. Stadelmaier³², D. Stanca⁷³, S. Stanič⁷⁶, J. Stasielak⁷⁰, P. Stassi³⁶, S. Strähnz³⁹, M. Straub⁴², M. Suárez-Durán¹⁴, T. Suomijärvi³⁷, A.D. Supanitsky⁷, Z. Svozilikova³², Z. Szadkowski⁷¹, A. Tapia²⁹, C. Taricco^{63,52}, C. Timmermans^{81,80}, O. Tkachenko⁴¹, P. Tobiska³², C.J. Todero Peixoto¹⁸, B. Tomé⁷², Z. Torrès³⁶, A. Travaini¹⁰, P. Travnicek³², C. Trimarelli^{57,46}, M. Tueros³, M. Unger⁴¹, L. Vaclavek³³, M. Vacula³³, J.F. Valdés Galicia⁶⁸, L. Valore^{60,50}, E. Varela⁶⁴, A. Vásquez-Ramírez³⁰, D. Veberič⁴¹, C. Ventura²⁷, I.D. Vergara Quispe³, V. Verzi⁵¹, J. Vicha³², J. Vink⁸³, J. Vlastimil³², S. Vorobiov⁷⁶, C. Watanabe²⁶, A.A. Watson^c, A. Weindl⁴¹, L. Wiencke⁸⁵, H. Wilczyński⁷⁰, D. Wittkowski³⁸, B. Wundheiler⁷, B. Yue³⁸, A. Yushkov³², O. Zapparrata¹⁴, E. Zas⁷⁹, D. Zavrtanik^{76,77}, M. Zavrtanik^{77,76}

-
- ¹ Centro Atómico Bariloche and Instituto Balseiro (CNEA-UNCuyo-CONICET), San Carlos de Bariloche, Argentina
² Departamento de Física and Departamento de Ciencias de la Atmósfera y los Océanos, FCEyN, Universidad de Buenos Aires and CONICET, Buenos Aires, Argentina
³ IFLP, Universidad Nacional de La Plata and CONICET, La Plata, Argentina
⁴ Instituto de Astronomía y Física del Espacio (IAFE, CONICET-UBA), Buenos Aires, Argentina
⁵ Instituto de Física de Rosario (IFIR) – CONICET/U.N.R. and Facultad de Ciencias Bioquímicas y Farmacéuticas U.N.R., Rosario, Argentina
⁶ Instituto de Tecnologías en Detección y Astropartículas (CNEA, CONICET, UNSAM), and Universidad Tecnológica Nacional – Facultad Regional Mendoza (CONICET/CNEA), Mendoza, Argentina
⁷ Instituto de Tecnologías en Detección y Astropartículas (CNEA, CONICET, UNSAM), Buenos Aires, Argentina
⁸ International Center of Advanced Studies and Instituto de Ciencias Físicas, ECyT-UNSAM and CONICET, Campus Miguelete – San Martín, Buenos Aires, Argentina
⁹ Laboratorio Atmósfera – Departamento de Investigaciones en Láseres y sus Aplicaciones – UNIDEF (CITEDEF-CONICET), Argentina
¹⁰ Observatorio Pierre Auger, Malargüe, Argentina
¹¹ Observatorio Pierre Auger and Comisión Nacional de Energía Atómica, Malargüe, Argentina
¹² Universidad Tecnológica Nacional – Facultad Regional Buenos Aires, Buenos Aires, Argentina
¹³ University of Adelaide, Adelaide, S.A., Australia
¹⁴ Université Libre de Bruxelles (ULB), Brussels, Belgium
¹⁵ Vrije Universiteit Brussels, Brussels, Belgium
¹⁶ Centro Federal de Educação Tecnológica Celso Suckow da Fonseca, Petropolis, Brazil
¹⁷ Instituto Federal de Educação, Ciência e Tecnologia do Rio de Janeiro (IFRJ), Brazil
¹⁸ Universidade de São Paulo, Escola de Engenharia de Lorena, Lorena, SP, Brazil
¹⁹ Universidade de São Paulo, Instituto de Física de São Carlos, São Carlos, SP, Brazil
²⁰ Universidade de São Paulo, Instituto de Física, São Paulo, SP, Brazil
²¹ Universidade Estadual de Campinas, IFGW, Campinas, SP, Brazil
²² Universidade Estadual de Feira de Santana, Feira de Santana, Brazil
²³ Universidade Federal de Campina Grande, Centro de Ciencias e Tecnologia, Campina Grande, Brazil
²⁴ Universidade Federal do ABC, Santo André, SP, Brazil
²⁵ Universidade Federal do Paraná, Setor Palotina, Palotina, Brazil
²⁶ Universidade Federal do Rio de Janeiro, Instituto de Física, Rio de Janeiro, RJ, Brazil
²⁷ Universidade Federal do Rio de Janeiro (UFRJ), Observatório do Valongo, Rio de Janeiro, RJ, Brazil
²⁸ Universidade Federal Fluminense, EEIMVR, Volta Redonda, RJ, Brazil
²⁹ Universidad de Medellín, Medellín, Colombia
³⁰ Universidad Industrial de Santander, Bucaramanga, Colombia

- ³¹ Charles University, Faculty of Mathematics and Physics, Institute of Particle and Nuclear Physics, Prague, Czech Republic
- ³² Institute of Physics of the Czech Academy of Sciences, Prague, Czech Republic
- ³³ Palacky University, Olomouc, Czech Republic
- ³⁴ CNRS/IN2P3, IJCLab, Université Paris-Saclay, Orsay, France
- ³⁵ Laboratoire de Physique Nucléaire et de Hautes Energies (LPNHE), Sorbonne Université, Université de Paris, CNRS-IN2P3, Paris, France
- ³⁶ Univ. Grenoble Alpes, CNRS, Grenoble Institute of Engineering Univ. Grenoble Alpes, LPSC-IN2P3, 38000 Grenoble, France
- ³⁷ Université Paris-Saclay, CNRS/IN2P3, IJCLab, Orsay, France
- ³⁸ Bergische Universität Wuppertal, Department of Physics, Wuppertal, Germany
- ³⁹ Karlsruhe Institute of Technology (KIT), Institute for Experimental Particle Physics, Karlsruhe, Germany
- ⁴⁰ Karlsruhe Institute of Technology (KIT), Institut für Prozessdatenverarbeitung und Elektronik, Karlsruhe, Germany
- ⁴¹ Karlsruhe Institute of Technology (KIT), Institute for Astroparticle Physics, Karlsruhe, Germany
- ⁴² RWTH Aachen University, III. Physikalisches Institut A, Aachen, Germany
- ⁴³ Universität Hamburg, II. Institut für Theoretische Physik, Hamburg, Germany
- ⁴⁴ Universität Siegen, Department Physik – Experimentelle Teilchenphysik, Siegen, Germany
- ⁴⁵ Gran Sasso Science Institute, L'Aquila, Italy
- ⁴⁶ INFN Laboratori Nazionali del Gran Sasso, Assergi (L'Aquila), Italy
- ⁴⁷ INFN, Sezione di Catania, Catania, Italy
- ⁴⁸ INFN, Sezione di Lecce, Lecce, Italy
- ⁴⁹ INFN, Sezione di Milano, Milano, Italy
- ⁵⁰ INFN, Sezione di Napoli, Napoli, Italy
- ⁵¹ INFN, Sezione di Roma “Tor Vergata”, Roma, Italy
- ⁵² INFN, Sezione di Torino, Torino, Italy
- ⁵³ Istituto di Astrofisica Spaziale e Fisica Cosmica di Palermo (INAF), Palermo, Italy
- ⁵⁴ Osservatorio Astrofisico di Torino (INAF), Torino, Italy
- ⁵⁵ Politecnico di Milano, Dipartimento di Scienze e Tecnologie Aeroespaziali , Milano, Italy
- ⁵⁶ Università del Salento, Dipartimento di Matematica e Fisica “E. De Giorgi”, Lecce, Italy
- ⁵⁷ Università dell'Aquila, Dipartimento di Scienze Fisiche e Chimiche, L'Aquila, Italy
- ⁵⁸ Università di Catania, Dipartimento di Fisica e Astronomia “Ettore Majorana“, Catania, Italy
- ⁵⁹ Università di Milano, Dipartimento di Fisica, Milano, Italy
- ⁶⁰ Università di Napoli “Federico II”, Dipartimento di Fisica “Ettore Pancini”, Napoli, Italy
- ⁶¹ Università di Palermo, Dipartimento di Fisica e Chimica “E. Segrè”, Palermo, Italy
- ⁶² Università di Roma “Tor Vergata”, Dipartimento di Fisica, Roma, Italy
- ⁶³ Università Torino, Dipartimento di Fisica, Torino, Italy
- ⁶⁴ Benemérita Universidad Autónoma de Puebla, Puebla, México
- ⁶⁵ Unidad Profesional Interdisciplinaria en Ingeniería y Tecnologías Avanzadas del Instituto Politécnico Nacional (UPIITA-IPN), México, D.F., México
- ⁶⁶ Universidad Autónoma de Chiapas, Tuxtla Gutiérrez, Chiapas, México
- ⁶⁷ Universidad Michoacana de San Nicolás de Hidalgo, Morelia, Michoacán, México
- ⁶⁸ Universidad Nacional Autónoma de México, México, D.F., México
- ⁶⁹ Universidad Nacional de San Agustín de Arequipa, Facultad de Ciencias Naturales y Formales, Arequipa, Peru
- ⁷⁰ Institute of Nuclear Physics PAN, Krakow, Poland
- ⁷¹ University of Łódź, Faculty of High-Energy Astrophysics, Łódź, Poland
- ⁷² Laboratório de Instrumentação e Física Experimental de Partículas – LIP and Instituto Superior Técnico – IST, Universidade de Lisboa – UL, Lisboa, Portugal
- ⁷³ “Horia Hulubei” National Institute for Physics and Nuclear Engineering, Bucharest-Magurele, Romania
- ⁷⁴ Institute of Space Science, Bucharest-Magurele, Romania
- ⁷⁵ University Politehnica of Bucharest, Bucharest, Romania
- ⁷⁶ Center for Astrophysics and Cosmology (CAC), University of Nova Gorica, Nova Gorica, Slovenia
- ⁷⁷ Experimental Particle Physics Department, J. Stefan Institute, Ljubljana, Slovenia

- ⁷⁸ Universidad de Granada and C.A.F.P.E., Granada, Spain
⁷⁹ Instituto Galego de Física de Altas Enerxías (IGFAE), Universidade de Santiago de Compostela, Santiago de Compostela, Spain
⁸⁰ IMAPP, Radboud University Nijmegen, Nijmegen, The Netherlands
⁸¹ Nationaal Instituut voor Kernfysica en Hoge Energie Fysica (NIKHEF), Science Park, Amsterdam, The Netherlands
⁸² Stichting Astronomisch Onderzoek in Nederland (ASTRON), Dwingeloo, The Netherlands
⁸³ Universiteit van Amsterdam, Faculty of Science, Amsterdam, The Netherlands
⁸⁴ Case Western Reserve University, Cleveland, OH, USA
⁸⁵ Colorado School of Mines, Golden, CO, USA
⁸⁶ Department of Physics and Astronomy, Lehman College, City University of New York, Bronx, NY, USA
⁸⁷ Michigan Technological University, Houghton, MI, USA
⁸⁸ New York University, New York, NY, USA
⁸⁹ University of Chicago, Enrico Fermi Institute, Chicago, IL, USA
⁹⁰ University of Delaware, Department of Physics and Astronomy, Bartol Research Institute, Newark, DE, USA
⁹¹ University of Wisconsin-Madison, Department of Physics and WIPAC, Madison, WI, USA

^a Louisiana State University, Baton Rouge, LA, USA

^b also at University of Bucharest, Physics Department, Bucharest, Romania

^c School of Physics and Astronomy, University of Leeds, Leeds, United Kingdom

^d now at Agenzia Spaziale Italiana (ASI). Via del Politecnico 00133, Roma, Italy

^e Fermi National Accelerator Laboratory, Fermilab, Batavia, IL, USA

^f now at Graduate School of Science, Osaka Metropolitan University, Osaka, Japan

^g now at ECAP, Erlangen, Germany

^h Max-Planck-Institut für Radioastronomie, Bonn, Germany

ⁱ also at Kapteyn Institute, University of Groningen, Groningen, The Netherlands

^j Colorado State University, Fort Collins, CO, USA

^k Pennsylvania State University, University Park, PA, USA

Acknowledgments

The successful installation, commissioning, and operation of the Pierre Auger Observatory would not have been possible without the strong commitment and effort from the technical and administrative staff in Malargüe. We are very grateful to the following agencies and organizations for financial support:

Argentina – Comisión Nacional de Energía Atómica; Agencia Nacional de Promoción Científica y Tecnológica (ANPCyT); Consejo Nacional de Investigaciones Científicas y Técnicas (CONICET); Gobierno de la Provincia de Mendoza; Municipalidad de Malargüe; NDM Holdings and Valle Las Leñas; in gratitude for their continuing cooperation over land access; Australia – the Australian Research Council; Belgium – Fonds de la Recherche Scientifique (FNRS); Research Foundation Flanders (FWO); Brazil – Conselho Nacional de Desenvolvimento Científico e Tecnológico (CNPq); Financiadora de Estudos e Projetos (FINEP); Fundação de Amparo à Pesquisa do Estado de Rio de Janeiro (FAPERJ); São Paulo Research Foundation (FAPESP) Grants No. 2019/10151-2, No. 2010/07359-6 and No. 1999/05404-3; Ministério da Ciência, Tecnologia, Inovações e Comunicações (MCTIC); Czech Republic – Grant No. MSMT CR LTT18004, LM2015038, LM2018102, CZ.02.1.01/0.0/0.0/16_013/0001402, CZ.02.1.01/0.0/0.0/18_046/0016010 and CZ.02.1.01/0.0/0.0/17_049/0008422; France – Centre de Calcul IN2P3/CNRS; Centre National de la Recherche Scientifique (CNRS); Conseil Régional Ile-de-France; Département Physique Nucléaire et Corpusculaire (DNC-IN2P3/CNRS); Département Sciences de l'Univers (SDU-INSU/CNRS); Institut Lagrange de Paris (ILP) Grant No. LABEX ANR-10-LABX-63 within the Investissements d'Avenir Programme Grant No. ANR-11-IDEX-0004-02; Germany – Bundesministerium für Bildung und Forschung (BMBF); Deutsche Forschungsgemeinschaft (DFG); Finanzministerium Baden-Württemberg; Helmholtz Alliance for Astroparticle Physics (HAP); Helmholtz-Gemeinschaft Deutscher Forschungszentren (HGF); Ministerium für Kultur und Wissenschaft des Landes Nordrhein-Westfalen; Ministerium für Wissenschaft, Forschung und Kunst des Landes Baden-Württemberg; Italy – Istituto Nazionale di Fisica Nucleare (INFN); Istituto Nazionale di Astrofisica (INAF); Ministero dell'Università e della Ricerca (MUR); CETEMPS Center of Excellence; Ministero degli Affari Esteri (MAE), ICSC Centro Nazionale di Ricerca in High Performance Computing, Big Data

and Quantum Computing, funded by European Union NextGenerationEU, reference code CN_00000013; México – Consejo Nacional de Ciencia y Tecnología (CONACYT) No. 167733; Universidad Nacional Autónoma de México (UNAM); PAPIIT DGAPA-UNAM; The Netherlands – Ministry of Education, Culture and Science; Netherlands Organisation for Scientific Research (NWO); Dutch national e-infrastructure with the support of SURF Cooperative; Poland – Ministry of Education and Science, grants No. DIR/WK/2018/11 and 2022/WK/12; National Science Centre, grants No. 2016/22/M/ST9/00198, 2016/23/B/ST9/01635, 2020/39/B/ST9/01398, and 2022/45/B/ST9/02163; Portugal – Portuguese national funds and FEDER funds within Programa Operacional Factores de Competitividade through Fundação para a Ciência e a Tecnologia (COMPETE); Romania – Ministry of Research, Innovation and Digitization, CNCS-UEFISCDI, contract no. 30N/2023 under Romanian National Core Program LAPLAS VII, grant no. PN 23/21/01/02 and project number PN-III-P1-1.1-TE-2021-0924/TE57/2022, within PNCDI III; Slovenia – Slovenian Research Agency, grants P1-0031, P1-0385, I0-0033, N1-0111; Spain – Ministerio de Economía, Industria y Competitividad (FPA2017-85114-P and PID2019-104676GB-C32), Xunta de Galicia (ED431C 2017/07), Junta de Andalucía (SOMM17/6104/UGR, P18-FR-4314) Feder Funds, RENATA Red Nacional Temática de Astropartículas (FPA2015-68783-REDT) and María de Maeztu Unit of Excellence (MDM-2016-0692); USA – Department of Energy, Contracts No. DE-AC02-07CH11359, No. DE-FR02-04ER41300, No. DE-FG02-99ER41107 and No. DE-SC0011689; National Science Foundation, Grant No. 0450696; The Grainger Foundation; Marie Curie-IRSES/EPLANET; European Particle Physics Latin American Network; and UNESCO.